VERTICAL-LIFT AIRCRAFT: AN APPLICATION OF COMPUTATIONAL FLUID DYNAMICS TO A VTOL ENGINE MODEL

An Undergraduate Research Scholars Thesis

by

LAMEES IBRAHIM ELNIHUM

Submitted to Honors and Undergraduate Research
Texas A&M University
in partial fulfillment of the requirements for the designation as an

UNDERGRADUATE RESEARCH SCHOLAR

Approved by
Research Advisor: Dr. Mark Holtzapple

May 2015

Major: Chemical Engineering

TABLE OF CONTENTS

ABSTRACT

Vertical-Lift Aircraft: An Application of Computational Fluid Dynamics to a VTOL Engine Model. (May 2015)

Lamees Ibrahim Elnihum
Department of Chemical Engineering
Texas A&M University

Research Advisor: Dr. Mark Holtzapple
Department of Chemical Engineering

Traditional VTOL aircraft engines use thrusts of air to lift the aircraft straight up and allow them to hover, take off, and land vertically. In this enhanced vertical lift engine design, the direction of incoming air flow is altered so that the accumulation of lift is mathematically proven to be significantly increased relative to that of the traditional VTOL engine. This improved lift is to be verified with software in computational fluid dynamics (CFD) herein. We will then use CFD software further to expand upon this design and optimize its structure and parameters for improved lift. With time, this technology could allow for vertical lift aircraft to become a part of our everyday life, with persons utilizing personal flight vehicles for transportation on a daily basis.

DEDICATION

To Amier, a thirteen-year-old Tasmanian devil whose inquisitive mind and boundless curiosity I pray will color his life as he grows from a boy into a man. I hope you never stop asking questions; I hope you find a wealth of passion, knowledge and power in your academic and personal pursuits; and I hope you set goals and cross milestone after milestone as you conquer the stars while reaching for the moon. May God give you happiness, contentment, and success.

Si aún está en tu mente, vale la pena correr el riesgo.

If it's still in your mind, it is worth taking the risk.

Paulo Coelho, *The Alchemist*

ACKNOWLEDGMENTS

I would like to thank the brilliant inventor Dr. Mark Holtzapple for allowing me to set foot into research when I first joined his biofuels research team two years ago. Thank you for your continued faith in my efforts to pursue this aeronautical idea that has been on your mind for years. I would also like to thank Nirupama Gopalaswami and Sualeh Khurshid for taking the time to impart their invaluable knowledge and assistance to me during this project. I could not have completed this thesis without you.

CHAPTER I

INTRODUCTION

Traditional vertical take-off and landing, or VTOL, aircraft employ engines that use thrusts of air to lift the aircraft straight up, thus allowing them to hover, take off, and land vertically. VTOL is a subset of STOVL, or short take-off and vertical landing. VTOL aircraft include those using a power rotor, such as helicopters and tiltrotors, as well as those using directed jet thrust, which typically remain fixed-wing during flight. VTOL aircraft generally move horizontally along the runway before taking off using vertical thrust, which ensures dual aerodynamic and thrust lift during take-off. This dual lift allows for aircraft to take off more efficiently and with heavier loads that are much lighter upon landing due to loss of propellant weight. For helicopters and some specialized fixing-wing aircraft (such as the VTOL Harrier), no runway is needed.

Figure 1 below illustrates the traditional transfer of air through the engine of a VTOL aircraft, the Yak-38, in the generation of vertical thrust for lift-off. The fans of jet-powered aircraft such as the Yak-38 generally face the oncoming airflow in line with the direction of flight, as illustrated in Figure 2 below. In a jet engine, air is sucked in by large fans at the front of the engine. Most of this air immediately bypasses the engine as exhaust and contributes to the majority of the thrust, while the remaining air is compressed by blades rotating at high speeds. In the engine core, fuel is burned in the combustion chamber to heat the air. The hot air expands and is pushed out through the exhaust nozzles, which can turn to different positions and force, or direct, gases either backward or downward.

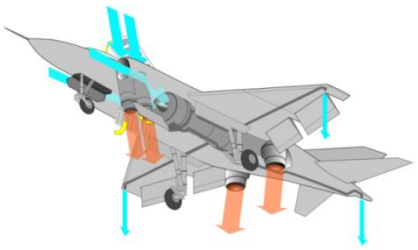

Figure 1 Diagram of the air forces on a VTOL aircraft, the Yakovlev Yak-38[1]

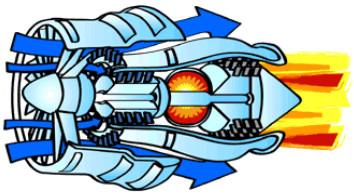

Figure 2 Illustration of air flow through a VTOL engine[2]

One of the most famous and successful VTOL aircraft is the Harrier Jump Jet, a subsonic attack aircraft powered by a single Rolls-Royce Pegasus turbofan engine, as displayed in Figure 3 below. The Pegasus 11-61 is the most powerful version of the engine and provides up to 23,800 lb_f (106 kN) of thrust lift. Because the weight of the aircraft exceeds the engine thrust when the Harrier is fully loaded with fuel and weapons, the Harrier is also known as a STOVL aircraft, meaning that a short sprint on the runway is needed to gain forward speed and aerodynamic lift before the aircraft can take off (saving fuel is also an additional benefit of this short sprint).

Figure 3 Rolls Royce Pegasus[3]

As of late 2010, the Harrier is intended to be replaced by the STOVL variant of the F-35 Lightning II, which employs the novel Rolls-Royce LiftSystem propulsion system as depicted in Figure 4 below. The LiftSystem generates thrust in the LiftFan and redirects the thrust from the main engine through the 3 Bearing Swivel Module and Roll Post ducts via the driveshaft. The result is a total of 41,900 lb_f (186 kN) of thrust lift, nearly twice that of the Harrier.

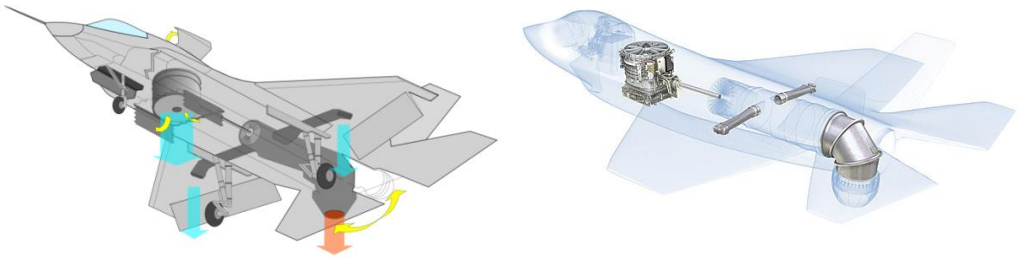

Figure 4 Rolls Royce LiftSystem[4,5]

The fact that the LiftFan is positioned at 90 degrees to the direction of oncoming airflow (unlike typical aircraft fans that face the oncoming airflow) produced a challenge that was addressed using the most advanced experimental and modeling techniques, including world-class computational fluid dynamics methods. An illustration of computational fluid flow across an aircraft is shown in Figure 5 below.

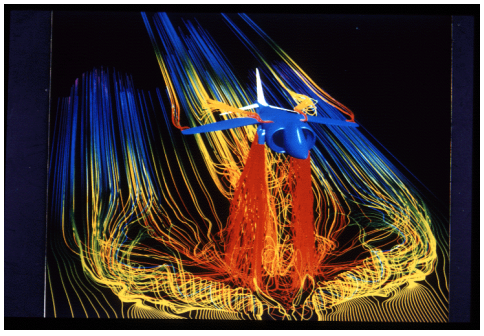

Figure 5 Illustration of CFD computations applied to the Harrier[6]

In traditional VTOL engines, air flows into the engine horizontally as the vehicle speeds through the atmosphere (or, in the case of the LiftSystem, enters vertically through the LiftFan). In our enhanced design, we propose an alternate engine scheme based on the theories below.

Thrust is a reaction force that is caused when a system expels or accelerates mass in one direction. The expelled mass will cause a force of equal magnitude but opposite direction on that system. An aircraft generates forward thrust when air is pushed in the direction opposite to flight.

If we point the positive x-direction towards the right relative to the engine lying on its side, as illustrated in Figure 6 below, the net accumulation of thrust is as follows:

$$Accumulation = Input - Output + Generation - Consumption \quad (1)$$

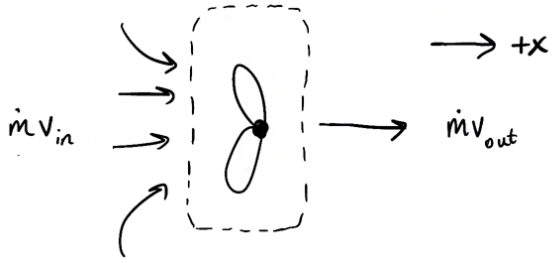

Figure 6 Traditional VTOL engine thrust accumulation

where generation and consumption are assumed to be zero. Employing the conservation of momentum to this equation, and referring to Figure 6, we can see that the input momentum is mv_{in} (a positive value) while the output momentum is mv_{out} (also a positive value). With force being the time rate of change of momentum, our final accumulation is

$$Accumulation = \dot{m}v_{in} - \dot{m}v_{out} \quad (2)$$

where the value of mv_{in} is small relative to the value of mv_{out}, and the accumulation term is negative. Thrust consequently occurs in the negative x-direction, inducing flight.

In our enhanced VTOL engine design, the magnitude of accumulation is considerably larger.

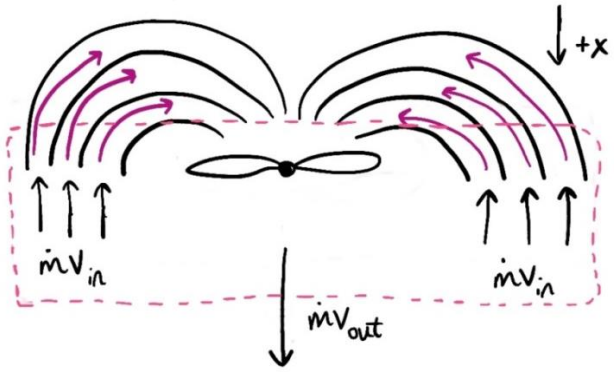

Figure 7 Enhanced VTOL engine thrust accumulation

If we point the positive x-direction downwards relative to the right-side up engine, as illustrated in Figure 7 above, the net accumulation is as follows:

$$Accumulation = Input - Output + Generation - Consumption \quad (1)$$

where generation and consumption are assumed to be zero. Employing the conservation of momentum to this equation, and referring to Figure 7, we can see that the input momentum is mv_{in} (a negative value) while the output momentum is mv_{out} (a positive value). Our final accumulation is thus

$$Accumulation = (-\dot{m}v_{in}) - \dot{m}v_{out} \quad (3)$$

where the accumulation is effectively doubled relative to that of the traditional VTOL engine. This research project aims to verify our hypothesis of an improved engine design based on our previous analysis and calculations. Our design of the vehicle is such that it is of standard

automobile size and implements retractable wings, so that the vehicle itself with its wings tucked in could be stored in a garage or storage area much like an everyday car. Such a design could allow for improved vertical aircraft design and potentially pave the way for a world in which people would have their own flight vehicles for transportation above ground level.

The general thrust equation is

$$F = \dot{m}v \tag{4}$$

and the general power equation is

$$P = \tfrac{1}{2}\,\dot{m}v^2 \tag{5}$$

Where aircraft are heavy vehicles with narrow air inlets and high-velocity air jets, our proposal offers a lightweight composite material design that retains a wide air intake. A larger inlet mass flow rate as allowed by these wider inlets allows for a smaller intake velocity. Although the intake velocity is smaller, the generated power is likely to remain sufficient for lift as this squared velocity term is paired with a greater mass influx. Thus we have magnitudes of mass flow rate and velocity suitable for lift while maintaining a velocity small enough for domestic use, i.e., this vehicle could be parked in a home garage and started in the driveway similar to a motor vehicle. The estimated energy usage of this design is twenty to thirty horsepower, where the average cruising motor vehicle utilizes approximately twenty horsepower. It should be noted that the weight of our vehicle will be significantly lower than that of the average motor vehicle. Also, the retractable wings will direct the course of the vehicle rather than rotating nozzles.

In a turbofan engine, as much as 75 percent of the total thrust may be attributed to the fan[7], as a portion of the inlet air that enters the fan is bypassed around the engine as exhaust (other engine

parts include the compressor, combustor, turbine, mixer and nozzle, as seen in Figure 8 below). Therefore in this analysis we will attribute thrust generation to the fan for simplicity, although the entirety of the engine can be modeled in CFD software and the effects of the fuel-utilizing engine parts studied (the fan may also be fuel-utilizing, or it may use electricity, power from the turbine, etc.). For example, if the nozzle had been modeled, the exit velocity as the air flow passes through the nozzle could be taken into account.

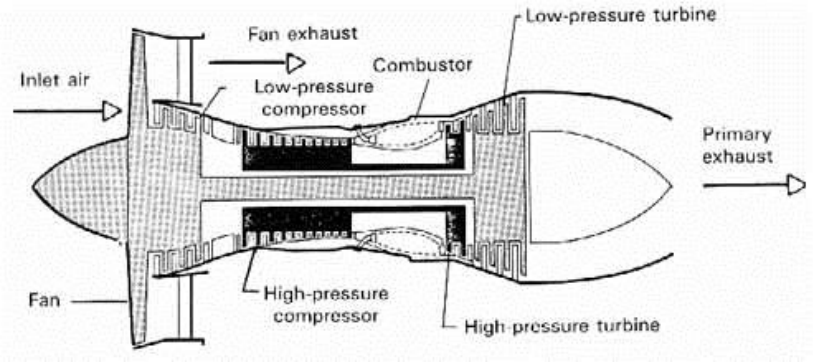

Figure 8 Turbofan engine schematic[7]

Because the design is symmetrical, only one-half of the engine will be modeled for simulation. The fan itself will not be modeled in CFD; rather, a vacuum pressure boundary condition will be applied at the ends of the modeled ducts in order to simulate the suction effects of the fan. Specifically, the pressure at the duct inlets will be atmospheric, and the pressure at the duct outlets will be set to a pressure low enough to generate a vacuum required for air suction.

Intuitively, to get the maximum efficiency of the proposed design, the velocity in each duct should be the same. In a frictionless environment, with each of the inlet pressures the same and each of the outlet pressures the same, this would imply that each of the ducts could have any

variable spacing. This derives from Bernoulli's law as displayed in Equation 6 below, which shows that the inlet and exit velocity of the air in the duct varies only with the pressure difference across the inlet and outlet for a steady and inviscid flow. Ducts of varying cross-sectional area with the same pressure difference across the inlet and outlet would have the same inlet and exit velocity. Here the inlet velocity is not a static zero as in a stationary engine, but the velocity at the inlet that results when this pressure difference is applied.

$$P_1 + \tfrac{1}{2}\rho v_1^2 = P_2 + \tfrac{1}{2}\rho v_2^2 \quad (6)$$

For a frictionless environment, the only way to increase flow velocity through a duct with a given pressure difference would be to decrease its cross-sectional area along its length.

However, in a viscous environment, friction would alter this setup. The presence of friction would require the duct thicknesses be altered in order to maintain the same outlet air velocity for each duct. This is because longer ducts will experience a greater amount of friction, which slows the flow down, due to the increased lengths of their inner walls. A wider cross-sectional area for longer ducts will input greater mass influx and ultimately allow for the same outlet velocity to be achieved while in the presence of greater friction. If the outlet velocities of each duct are not equivalent, a moment would be generated and undesired rotation of the engine would occur.

The objective of this analysis is to find spacings such that the outlet velocity is the same in each duct for the same pressure difference across the inlet and outlet. An initial duct spacing design will be modeled and simulated at varying vacuum pressures. The CFD results will indicate the velocities across the duct inlets and outlets. Then, additional spacing designs will be modeled and simulated at varying vacuum pressures as well. The compiled data will be used to generate a

graph of lift (in Newtons) versus vacuum pressure (in Pascals) for each duct spacing design, where the rate of change of mass with respect to time is defined as

$$\dot{m} = \rho A v \tag{7}$$

and lift is calculated as

$$Lift = Thrust = \dot{m}v = \rho A v^2 \tag{8}$$

Air density is known as 1.225 kg/m^3 and outlet velocity is found via CFD simulation. The lift found here will be multiplied by two in order to account for the mirroring half of the engine design.

It is our belief that the maximum lift as displayed on the graphs will be attributed to a certain duct spacing design simulated at a certain vacuum pressure that allows for equivalent velocities at the duct outlets.

Finally, further design optimization can include altering the number of air ducts in the engine; the height and width of the outermost duct; etc.

CHAPTER II

METHODS

The program ANSYS FLUENT 14.0, a component of ANSYS CFD software that allows engineers to simulate fluid flow in a virtual environment, was used to accomplish this project. The integration of ANSYS FLUENT into ANSYS Workbench allowed modeling and meshing with ANSYS DesignModeler and ANSYS Meshing, respectively.

ANSYS DesignModeler

For the initial guess of the optimal number of ducts in the design, four ducts for an approximately four-foot flow cross-section seemed reasonable. More ducts imply more friction due to increased surface area, while too few ducts would result in inefficient flow patterns. CFD simulation would ultimately provide a more definitive answer. When modeling the ducts, it is not necessary to extend the cross-section of the engine into the third dimension, as this would require extra computational power when little is happening in this dimension. A three-dimensional model created in ANSYS DesignModeler is shown in Figure 9 below for conceptual vision.

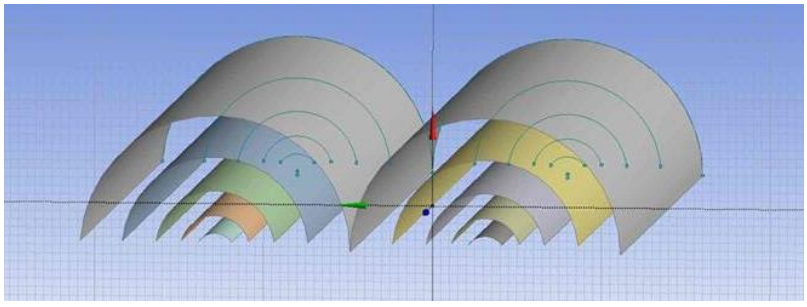

Figure 9 3-D conceptual engine model, cross-section extruded five meters

The dimensions of the average motor vehicle[8] were looked into so that a corresponding two-dimensional engine design could be sketched with similar length and width parameters; this diagram can be viewed in Appendix A. The height and width of the outermost duct is 0.8 meters and 1.6 meters, respectively. The initial design consisted of a duct spacing that increased in increments of 0.05 meters as the ducts grew longer. The dimensions are shown in Table 1 below.

Table 1 Initial engine design dimensions

Arc	First Point (m)	Second Point (m)	Third Point (m)	Duct Width (m)
L_1	(0, 0)	(0.8, 0.8)	(1.6, 0)	0.25 (Duct A_1)
L_2	(0.25, 0)	(0.8, 0.55)	(1.35, 0)	0.2 (Duct A_2)
L_3	(0.45, 0)	(0.8, 0.35)	(1.15, 0)	0.15 (Duct A_3)
L_4	(0.6, 0)	(0.8, 0.2)	(1.0, 0)	0.1 (Duct A_4)
L_5	(0.7, 0)	(0.8, 0.1)	(0.9, 0)	--

Arcs L_1 through L_5 are labeled along with other parameters in a sketch of the 2-D design as shown in Figure 10 below.

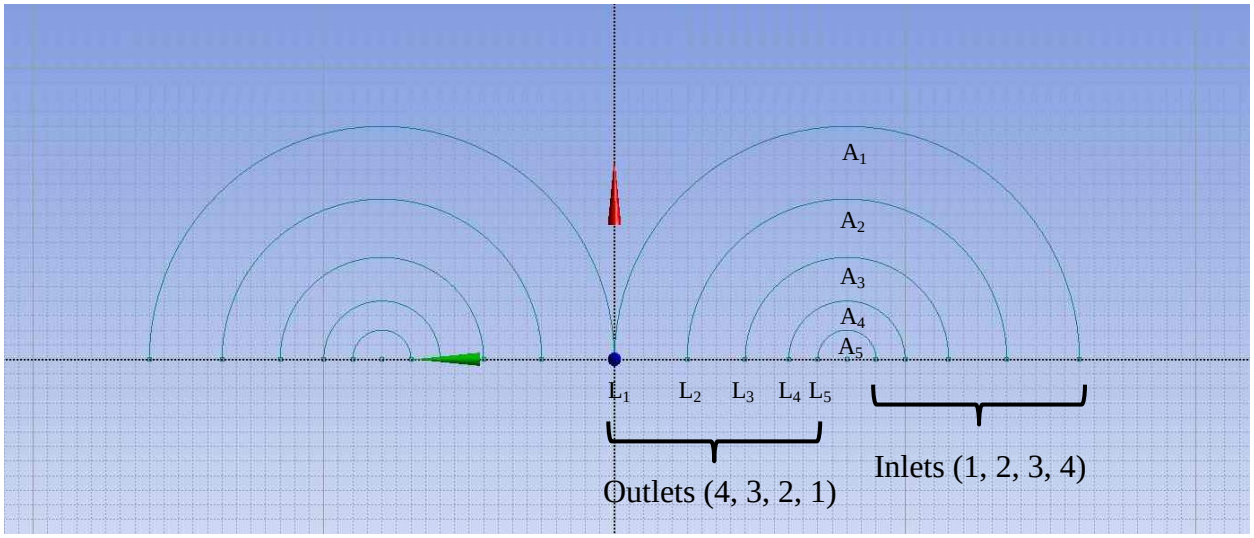

Figure 10 2-D engine design

Modeling the geometry in Fluent was undertaken. Because of the design symmetry, only the right half of the engine design was modeled. In DesignModeler, a total of thirteen sketches were drawn: Arcs L_1 through L_4, four inlets, four outlets, and a closed semicircle. A total of twelve line bodies were generated from the four arcs, four inlets, and four outlets. A total of five surface bodies were generated; four surface bodies for Ducts A_1 through A_4 (each defined as a fluid), and one for the closed semicircle (defined as a solid). This produced a total of seventeen bodies. A named selection was created for each of these seventeen bodies: Inlets 1 through 4, Outlets 1 through 4, Solid (referring to the closed semicircle), Walls 1 through 4 (referring to Arcs L_1 through L_4), and Fluids 1 through 4 (referring to Ducts A_1 through A_4). These seventeen bodies were then grouped together to create one part. The closed system could then be analyzed in ANSYS Meshing. The two-dimensional model can be seen in Figures 11 through 13 below.

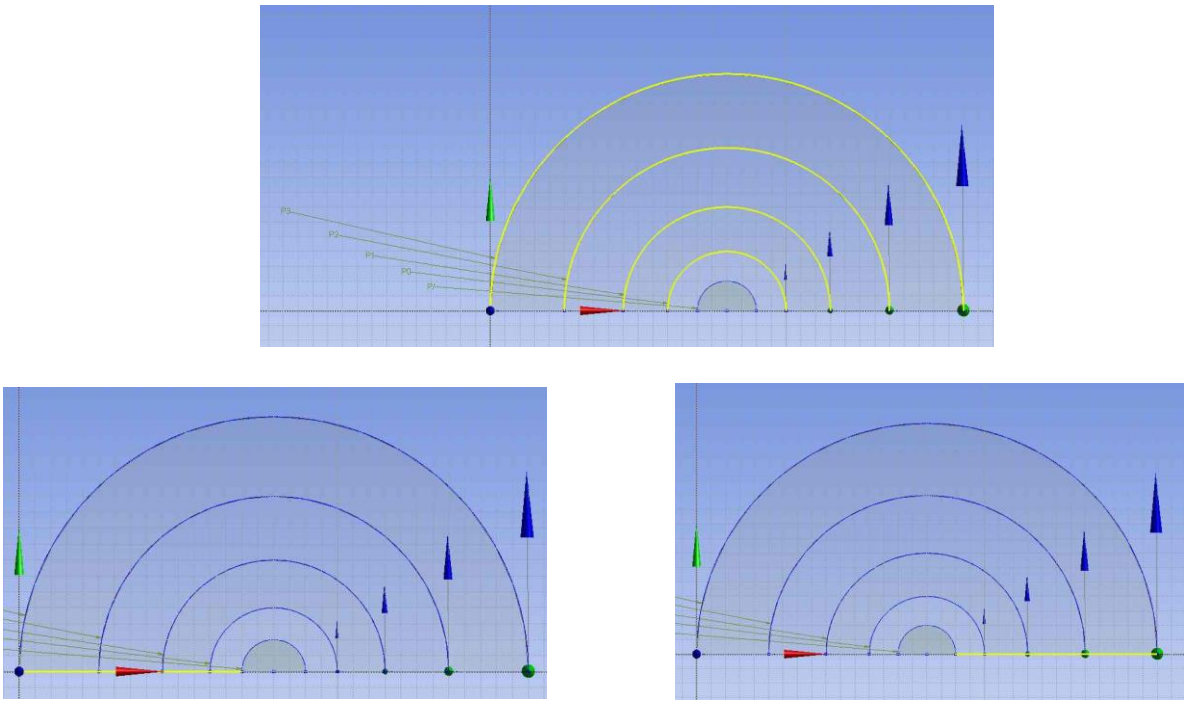

Figure 11 2-D design with Arcs L_2 through L_5 (top), Outlets 1 through 4 (bottom left left), and Inlets 1 through 4 highlighted

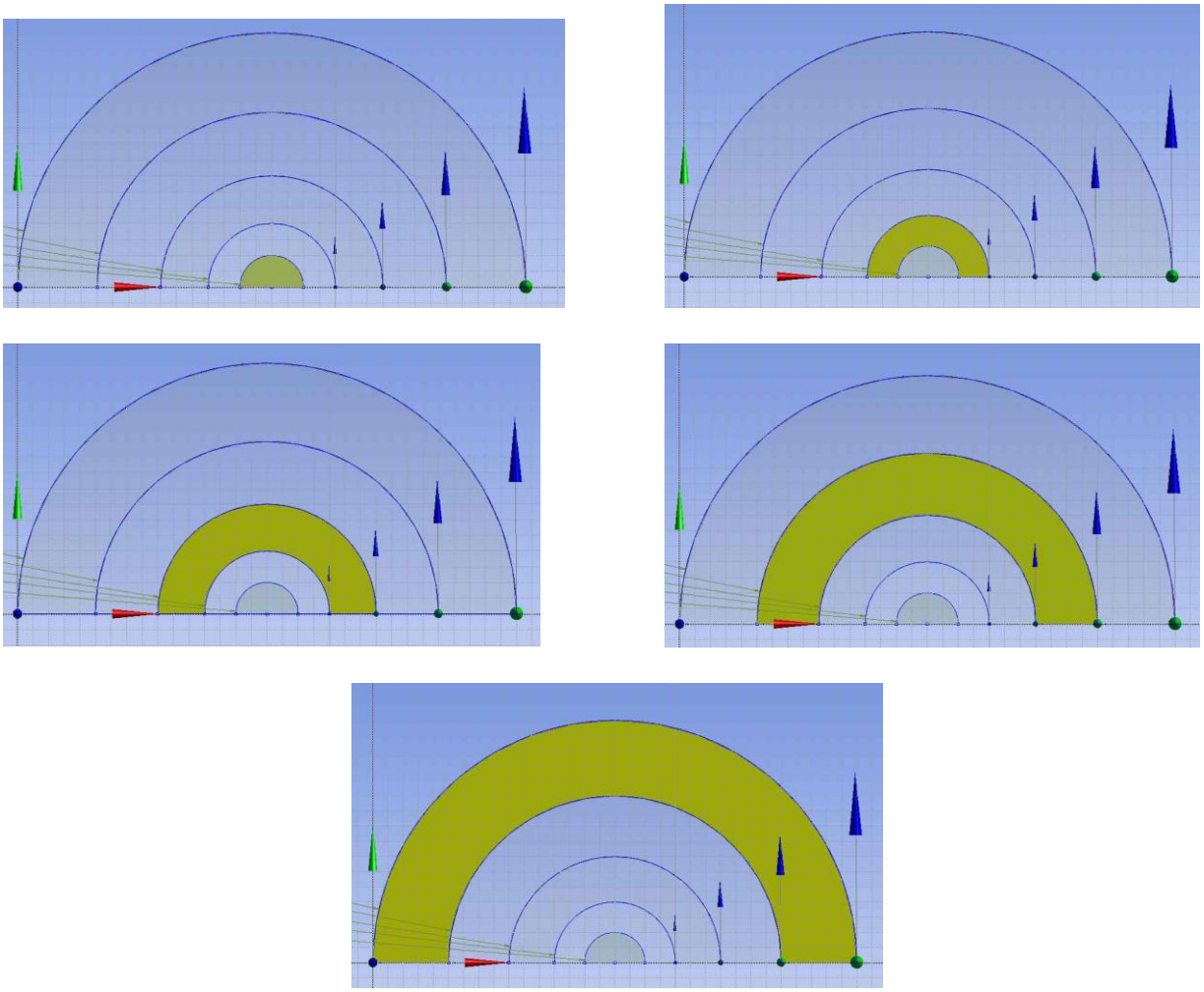

Figure 12 2-D design with Ducts A_1 through A_4 highlighted

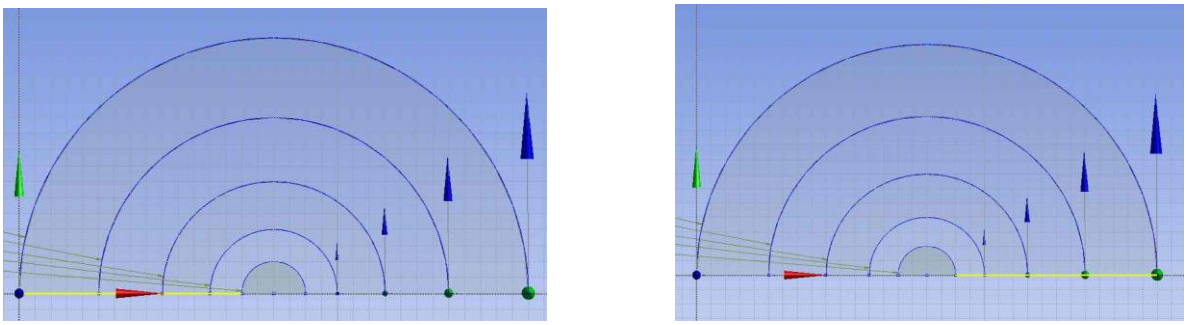

Figure 13 2-D design with Outlets 1 through 4 (left) and Inlets 1 through 4 highlighted

Design parameters were also set for the radii of Arcs L_1 through L_4 for later optimization of duct spacing.

Although this procedure has not yet been undertaken in this project, it should be noted that a good estimate of the duct spacing may be calculated by modeling the duct as a pipe. The pipe is modeled using the Fanning friction factor as given by the Churchill equation, which requires the input of a Reynolds number and therefore inlet or outlet velocities. Because the duct is non-circular, the geometry is modeled using the hydraulic diameter, as calculated in Table 2 below.

Table 2 Initial engine model hydraulic diameters

Modeling the Ducts as Semicircles	Semicircle Length (m)	Area (m^2)	Wetted Perimeter (m)	Hydraulic Diameter (m)
A_1	L_1 = 2.51	0.53	4.74	0.447
A_2	L_2 = 1.73	0.28	3.23	0.35
A_3	L_3 = 1.10	0.13	2.03	0.256
A_4	L_4 = 0.63	0.05	1.14	0.165
A_5	L_5 = 0.31	0.016	0.31	--

ANSYS Meshing

In Meshing, four line bodies (Walls 1 through 4) were defined as solid, while eight (Inlets 1 through 4 and Outlets 1 through 4) were defined as fluid. Four surface bodies (Fluids 1 through 4) were defined as fluid and one (Solid) was defined as solid.

Minimum Mesh sizing was set to 0.001 meters with the maximum at 0.002 meters. Relevance Center was set to Fine. The generated mesh is shown in Figure 14 below.

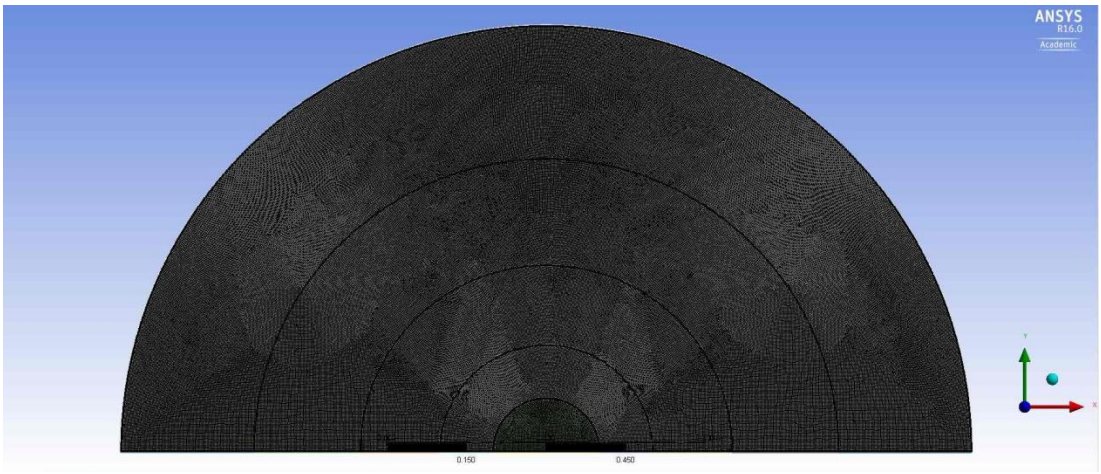

Figure 14 Meshing the 2-D model

ANSYS FLUENT

The simulation was treated as a steady (not transient) flow, both viscous and laminar. The solid was modeled as aluminum. The pressures at Inlets 1 through 4 were defined at 101,325 Pascals, or atmospheric pressure. The pressures at Outlets 1 through 4 were defined at an initial value of 50,000 Pascals.

CHAPTER III

RESULTS

The results for the simulation at a vacuum pressure of 50,000 Pascals are shown in Figure 15 below, illustrating the velocity contours of the fluid as it flows through the ducts.

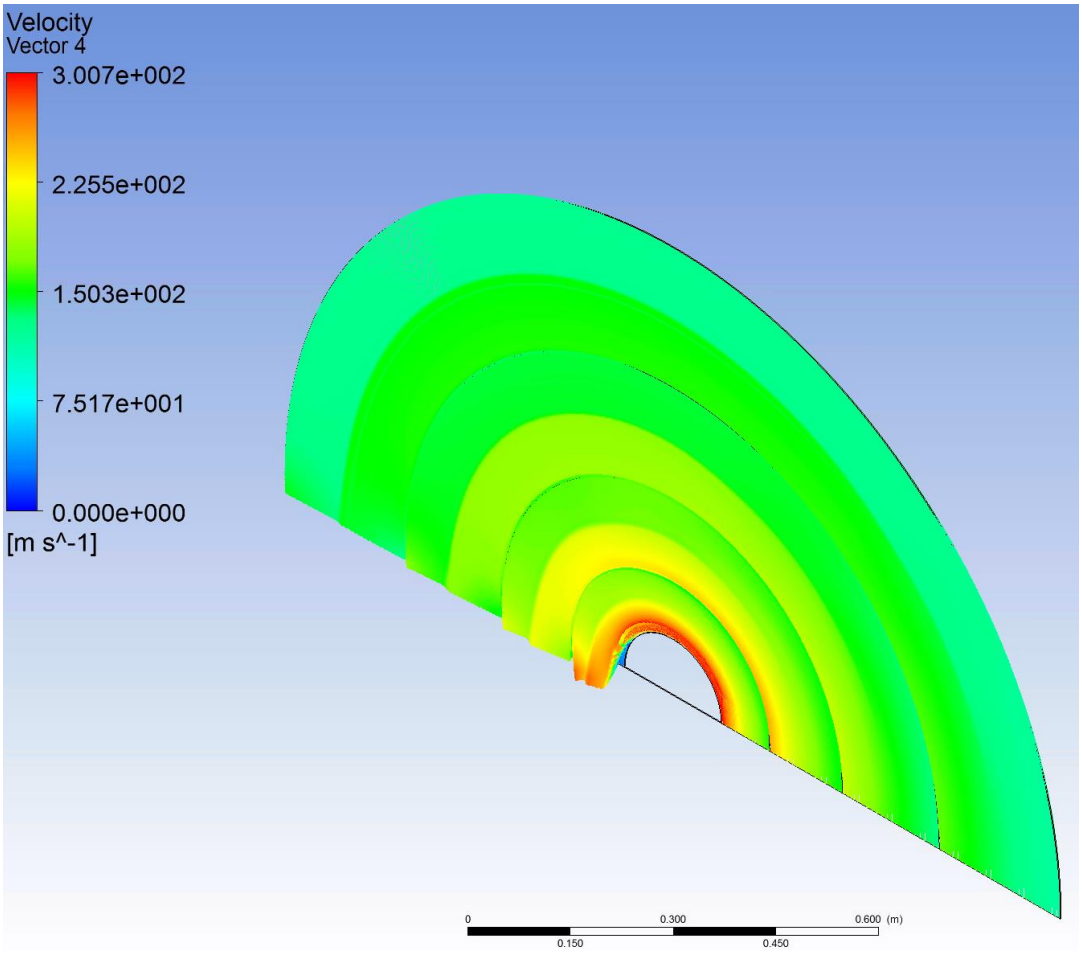

Figure 15 Velocity contours at a vacuum pressure of 50,000 Pascals

The inlet and outlet velocities versus inlet and outlet duct width are graphed for Ducts 1 through 4 in Figures 18 through 25 displayed in Appendix B.

The results for the simulation at a vacuum pressure of 10,000 Pascals are shown in Figure 16 below, illustrating the velocity contours of the fluid as it flows through the ducts.

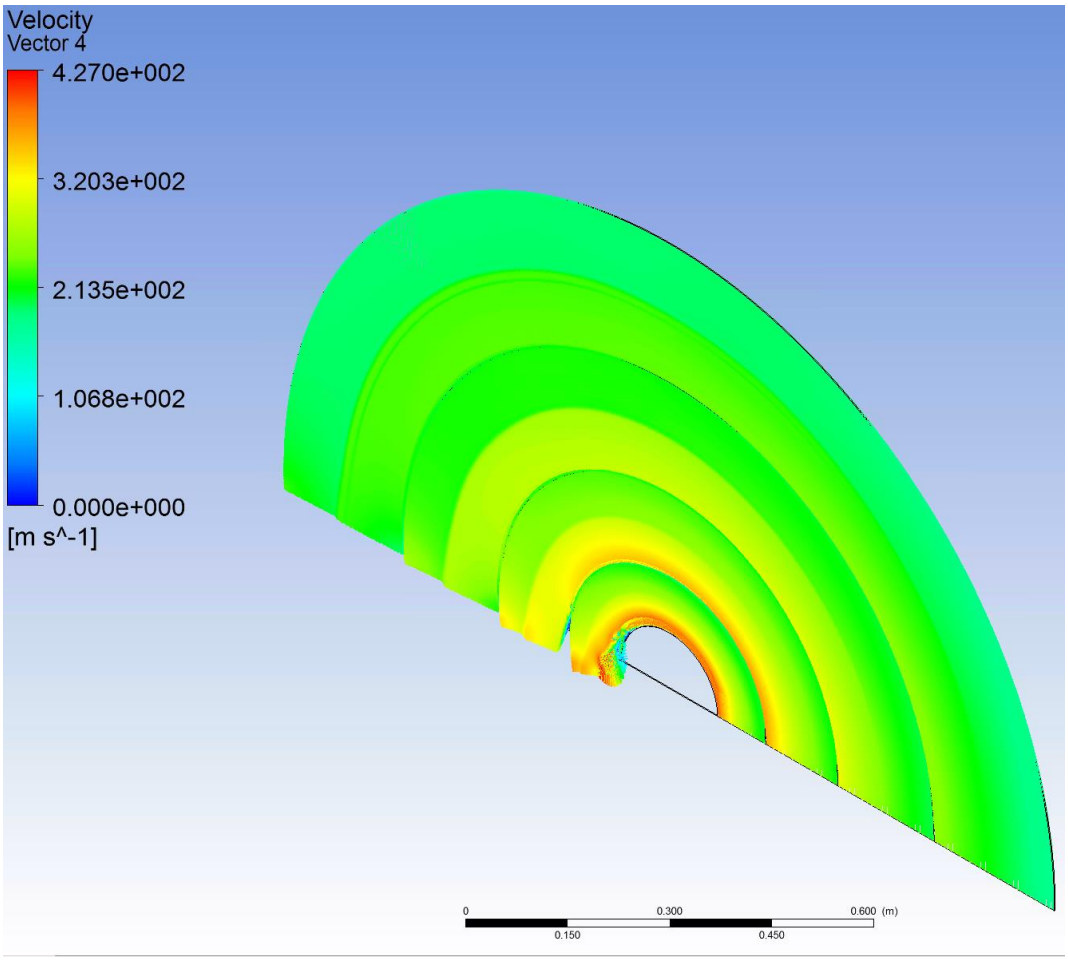

Figure 16 Velocity contours at a vacuum pressure of 10,000 Pascals

The inlet and outlet velocities versus inlet and outlet duct width are graphed for Ducts 1 through 4 in Figures 26 through 33 displayed in Appendix C.

The outlet velocities are not equivalent as ideally desired, but their magnitudes imply that the generation of lift looks promising. Therefore we obtain a rough approximation of lift for each

vacuum pressure using the maximum outlet velocities along with Equation 8, as shown in Table 3 below. Outlet areas are calculated for a unit span of one meter.

Table 3 Lift (N, lb_f) for the two simulations

	Vacuum pressure (Pascals)	
	50,000	10,000
Outlet 1 area, m^2	0.25	0.25
Outlet 1 velocity, m/s	150	220
Outlet 1 lift, N	6890	14,820
Outlet 2 area , m^2	0.2	0.2
Outlet 2 velocity, m/s	170	260
Outlet 2 lift, N	7080	16,560
Outlet 3 area, m^2	0.15	0.15
Outlet 3 velocity, m/s	210	330
Outlet 3 lift, N	8100	20,000
Outlet 4 area, m^2	0.1	0.1
Outlet 4 velocity, m/s	270	360
Outlet 4 lift, N	8930	15,900
Total lift, N	31,000	67,280
Total lift, N (engine span 5 meters)	155,000	336,400
Total lift, N (multiplication factor of 2)	62,000	134,560
Total lift, N (multiplication factor of 2, engine span 5 meters)	310,000	672,800
Total lift, lb_f	6970	15,125
Total lift, lb_f (engine span 5 meters)	34,850	75,625
Total lift, lb_f (multiplication factor of 2)	13,940	30,250
Total lift, lb_f (multiplication factor of 2, engine span 5 meters)	69,690	151,250

CHAPTER IV

CONCLUSIONS

The results obtained offer magnitudes of lift that encourage our theory of improved thrust via this design. Therefore, it is recommended to delve full force into this project and develop a table that charts lift in as a function of vacuum pressure for a series of spacing designs, in an attempt to find a design that provides equivalent outlet velocities for each duct (and in theory the most lift). A simplified example of such a chart is shown in Table 4 below.

Table 4 Lift (Newtons) versus vacuum pressure (Pascals)

Lift (Newtons)	Vacuum Pressure (Pascals)							
Spacing Design	10,000	20,000	30,000	40,000	50,000	60,000	70,000	80,000
1								
2								
3								
4								

In further analyses, the design parameters applied to the radii of arcs L_1 through L_4 will be implemented to find optimum spacing; also, the initial simulation results regarding inlet and outlet velocities can provide a starting point for use of the Fanning friction factor equation in initially estimating optimum duct spacing.

Lastly, in retrospect, it was not necessary to model the solid semicircle beneath the smallest arc.

REFERENCES

1. “Yakovlev Yak-38.” *Wikipedia.* Wikimedia Foundation, Inc., 2015. Web. 1 Jan. 2015. <http://en.wikipedia.org/wiki/Yakovlev_Yak-38>.

2. “How does a jet engine work?” *Glenn Research Center.* NASA, 2014. Web. 1 Jan. 2015. <http://www.grc.nasa.gov/WWW/k-12/UEET/StudentSite/engines.html>.

3. “Rolls-Royce Pegasus.” *Turbokart.com.* Turbokart, 2009. Web. 1 Jan. 2015. <http://www.turbokart.com/about_pegasus.htm>.

4. “Rolls-Royce LiftSystem.” *Wikipedia.* Wikimedia Foundation, Inc., 2015. Web. 1 Jan. 2015. <http://en.wikipedia.org/wiki/Rolls-Royce_LiftSystem>.

5. “Rolls-Royce LiftSystem.” *Rolls-Royce.* Rolls-Royce PLC, 2015. Web. 1 Jan. 2015. <http://www.rolls-royce.com/customers/defence-aerospace/products/combat-jets/rolls-royce-liftsystem.aspx>.

6. “NASA.” *NITRD*. NITRD, 2015. Web. 1 Jan. 2015. <https://www.nitrd.gov/pubs/bluebooks/1994/section.4.4.html>.

7. “Turbojet and Turbofan Systems.” *NASA Headquarters.* NASA, 2013. Web. 1 Jan. 2015. <http://www.hq.nasa.gov/pao/History/SP-468/ch10-3.htm>.

8. "Motoring." UK Metric Association, 2013. Web. 1 Jan. 2015. <http://www.metric.org.uk/motoring>.

APPENDIX A

	SALOON
A	2 815
B	1 054
C	910
D	4 779
E	1 586
F	2 096
G	1 557
H	1 860
I*	1 451

* Without roof bars.

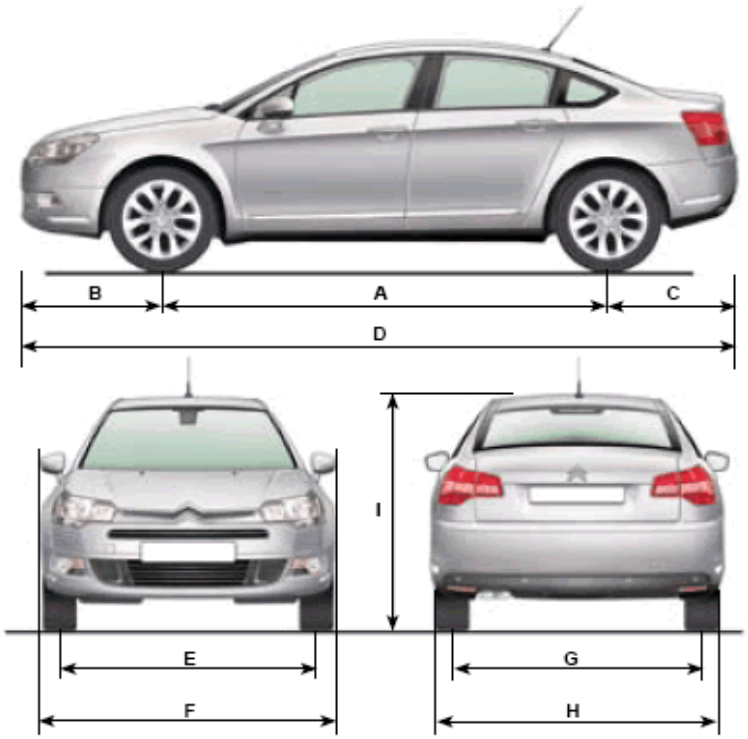

Figure 17 Motoring metrics[8]

APPENDIX B

Figure 18 Inlet 1, inlet velocity versus inlet length

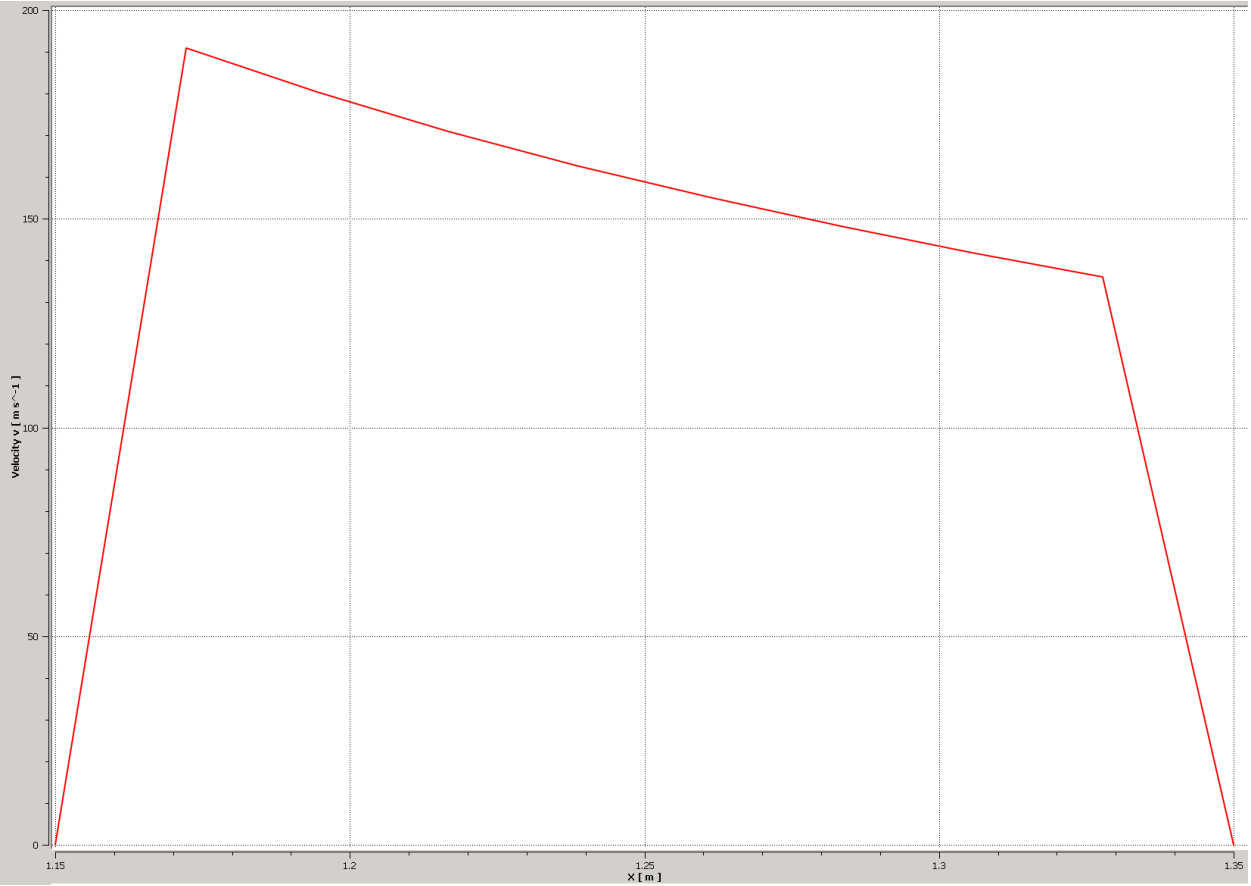

Figure 19 Inlet 2, inlet velocity versus inlet length

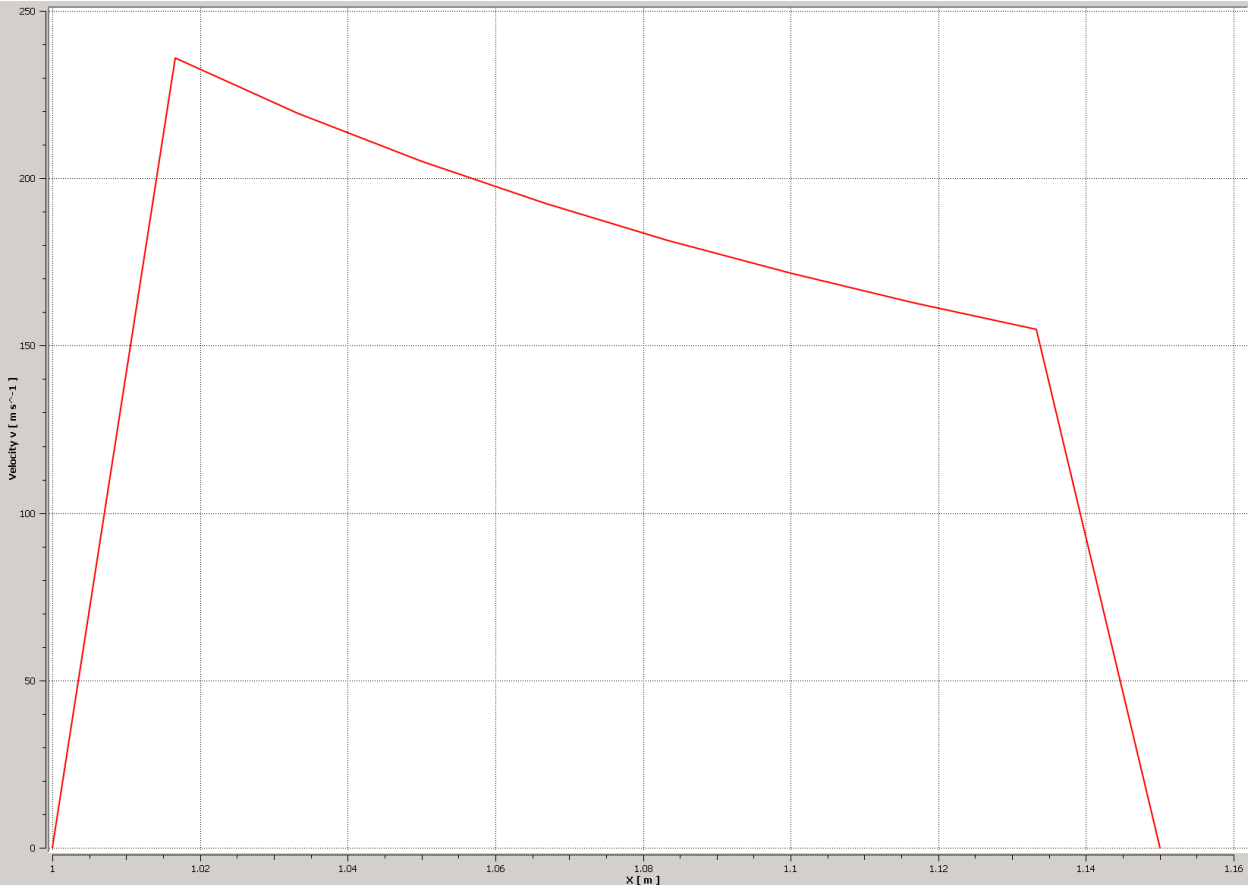

Figure 20 Inlet 3, inlet velocity versus inlet length

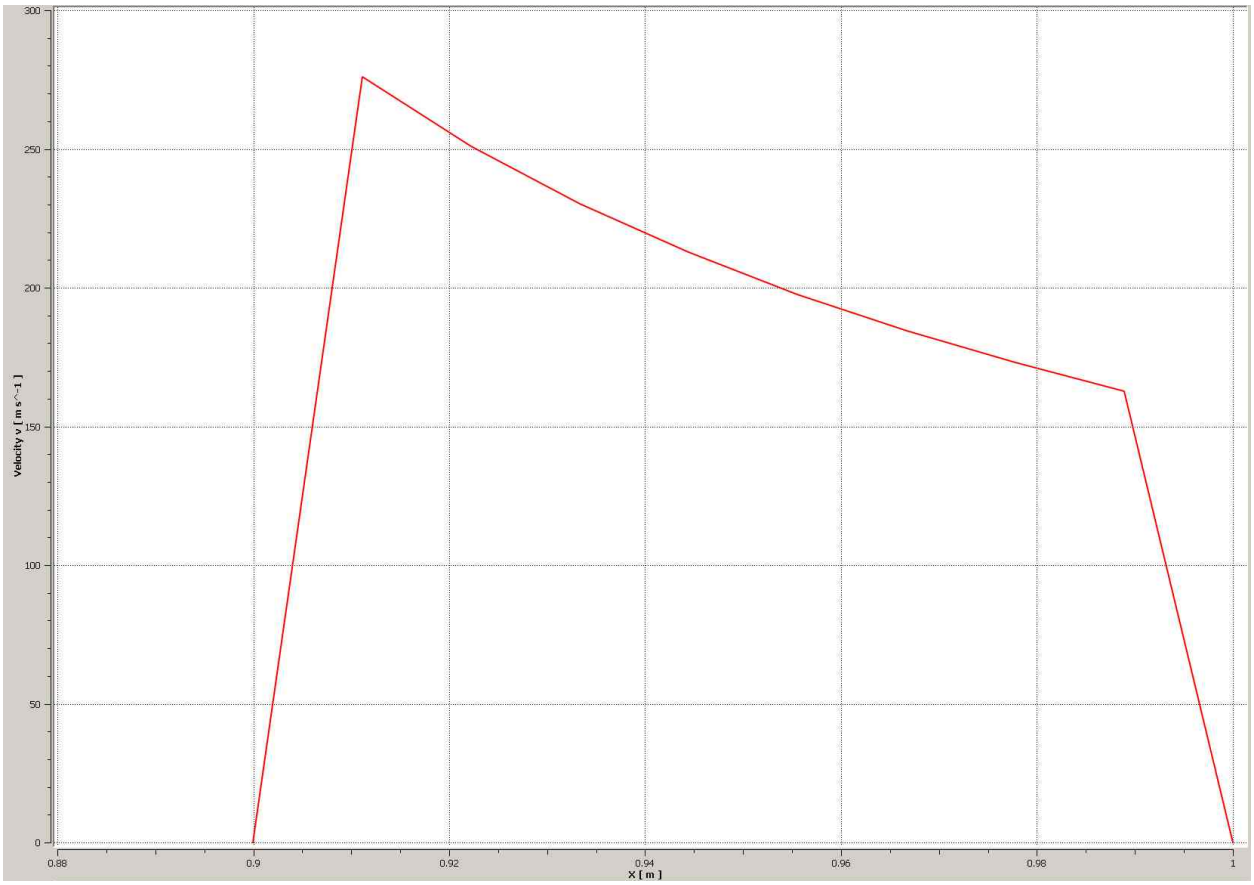

Figure 21 Inlet 4, inlet velocity versus inlet length

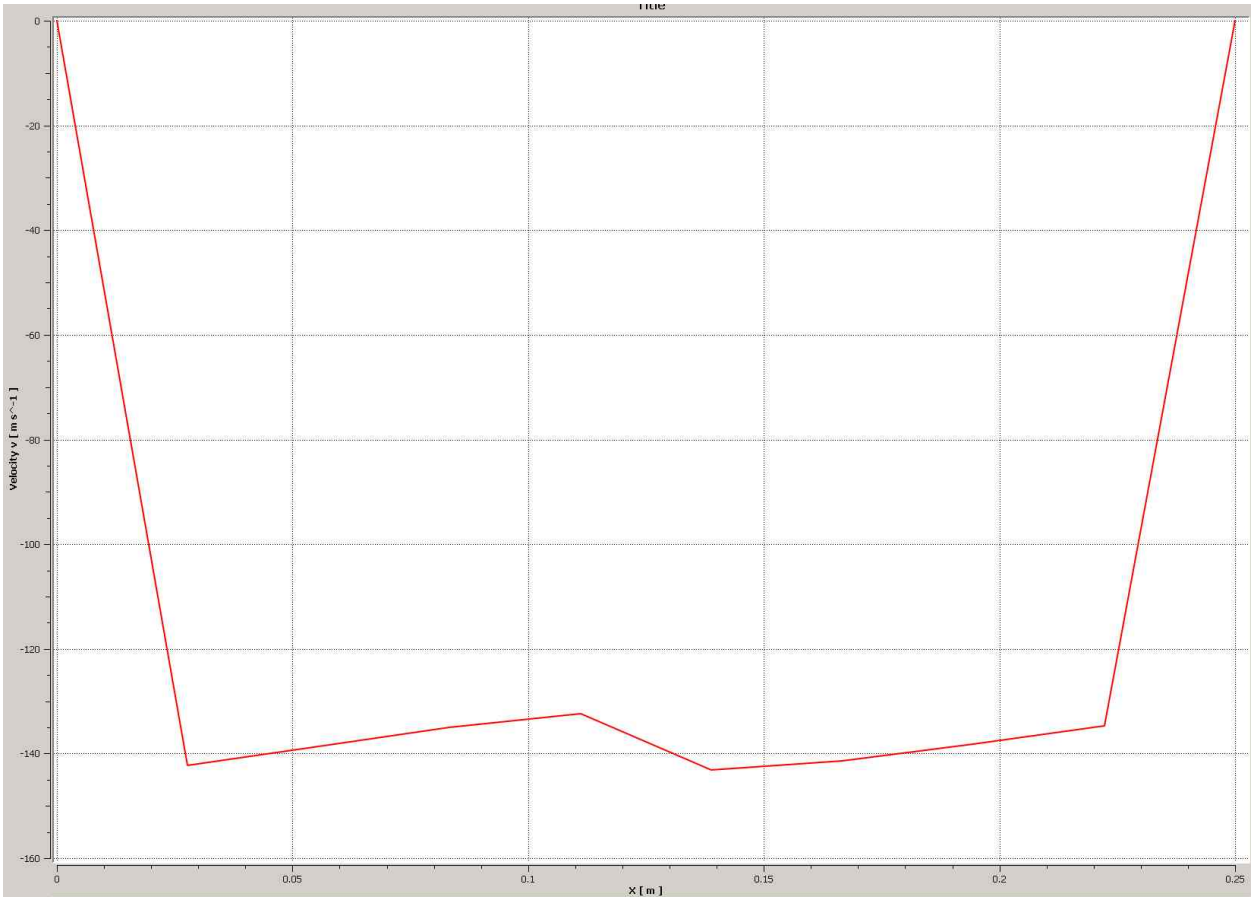

Figure 22 Outlet 1, outlet velocity versus outlet length

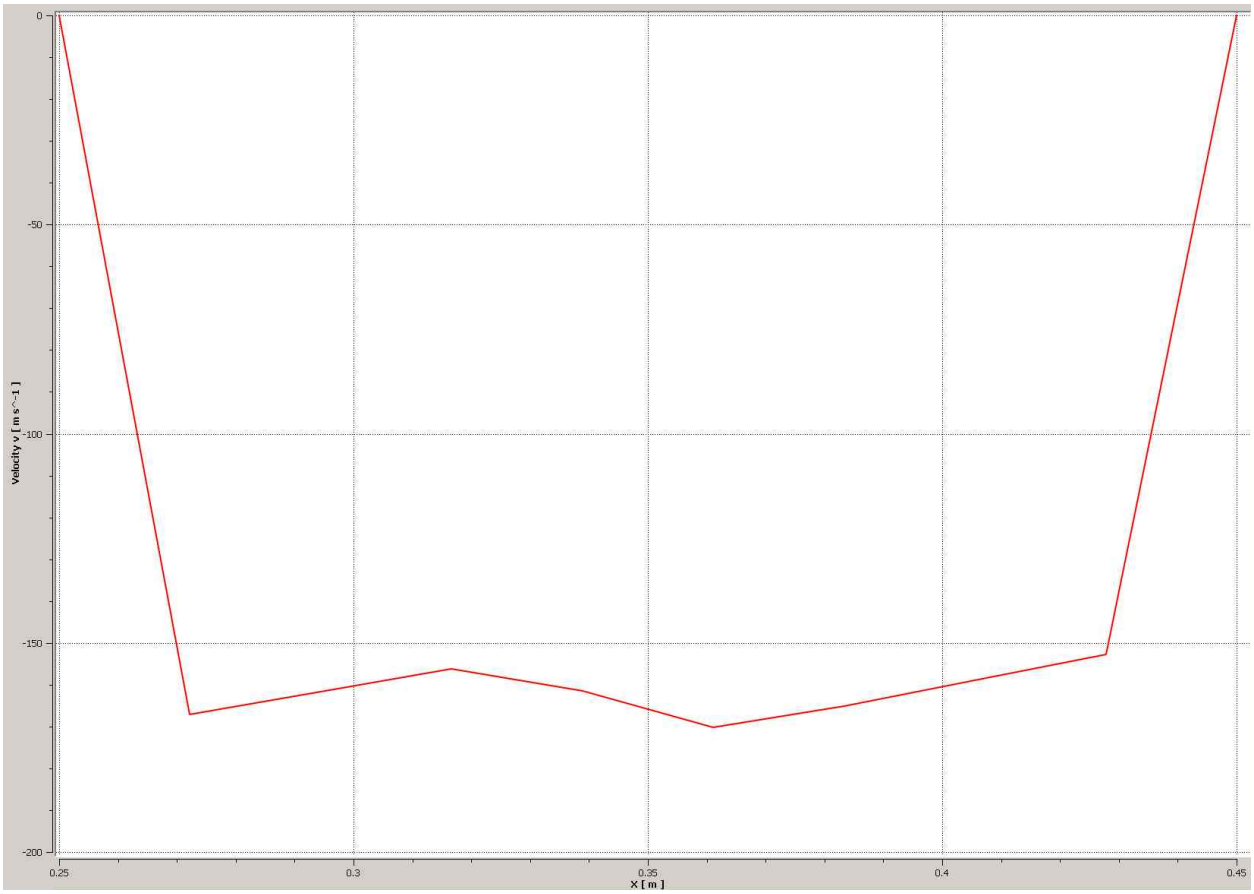

Figure 23 Outlet 2, outlet velocity versus outlet length

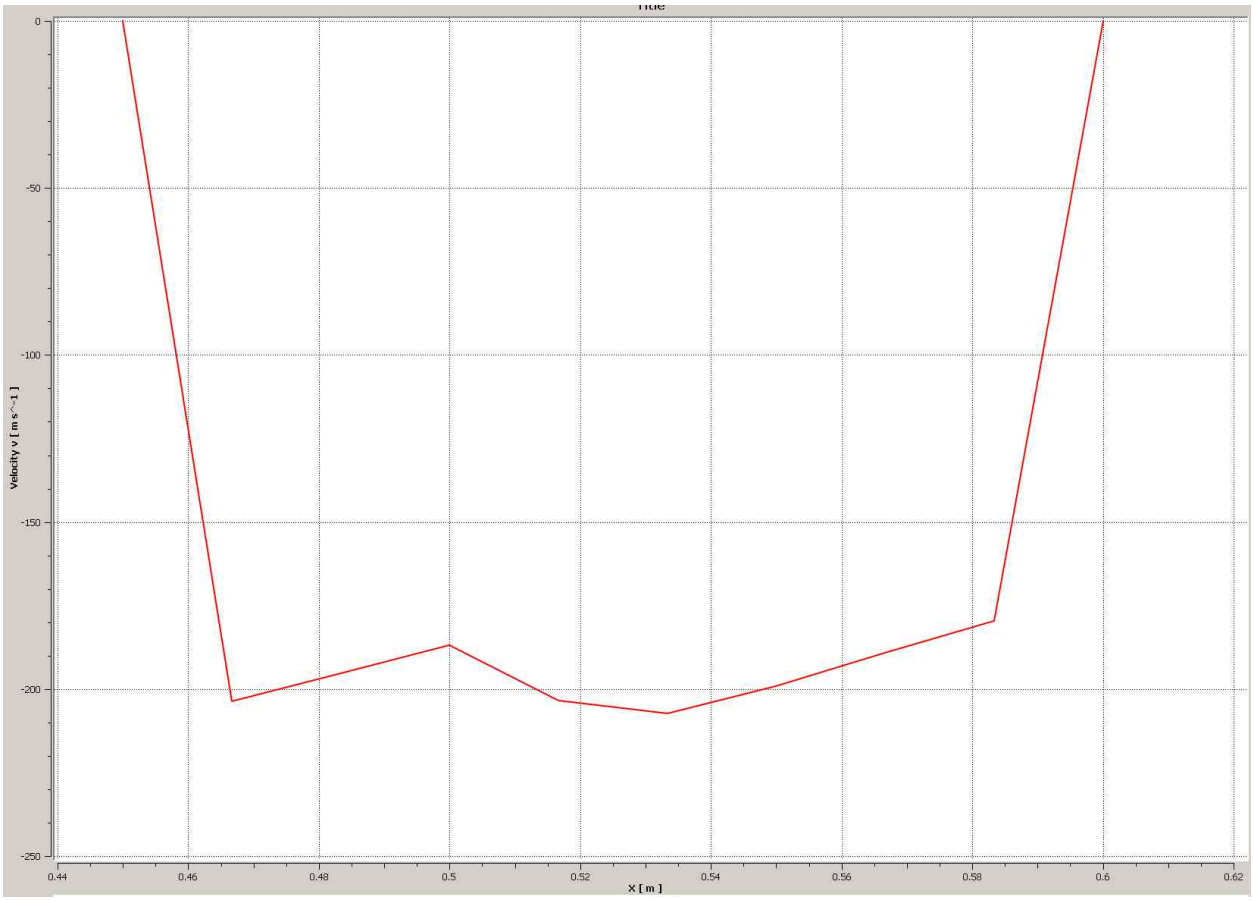

Figure 24 Outlet 3, outlet velocity versus outlet length

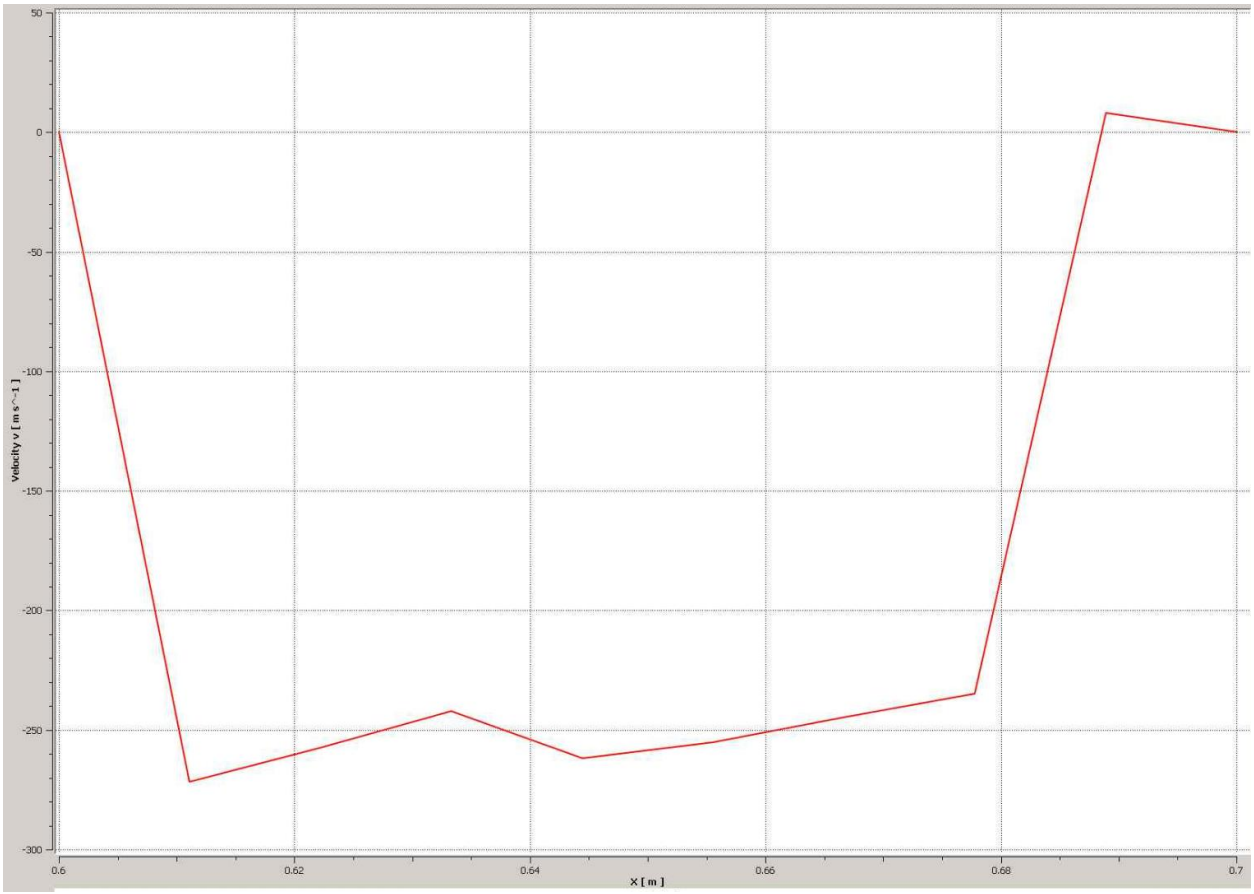

Figure 25 Outlet 4, outlet velocity versus outlet length

APPENDIX C

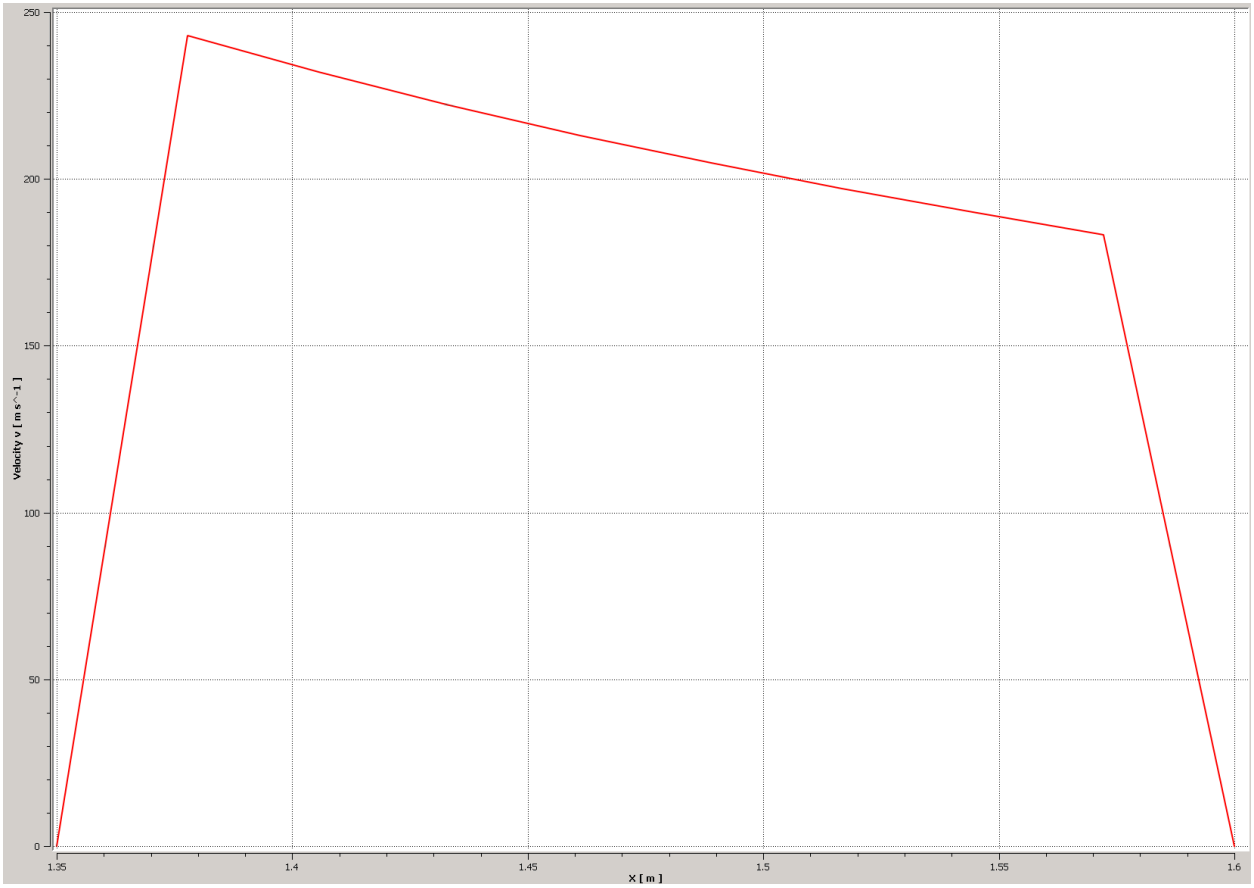

Figure 26 Inlet 1, inlet velocity versus inlet length

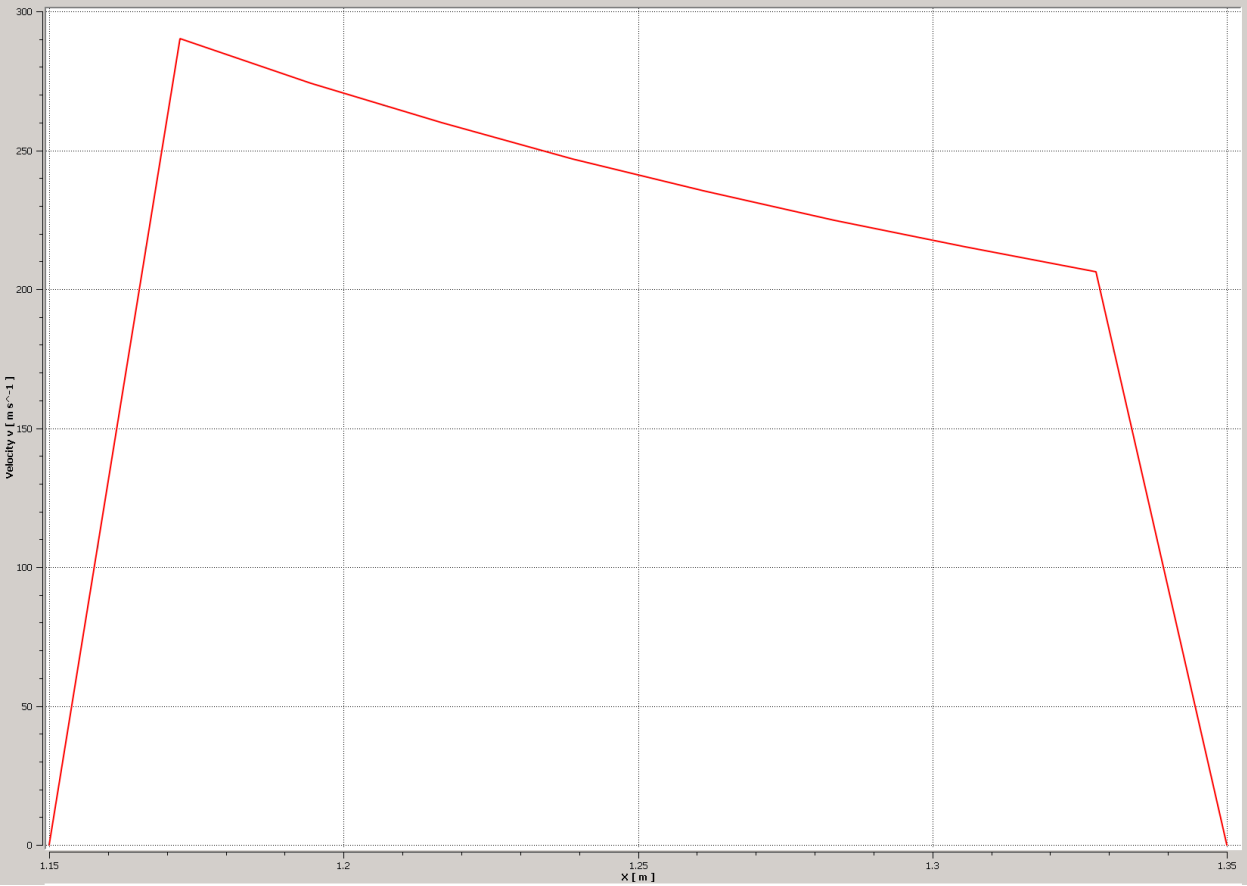

Figure 27 Inlet 2, inlet velocity versus inlet length

Figure 28 Inlet 3, inlet velocity versus inlet length

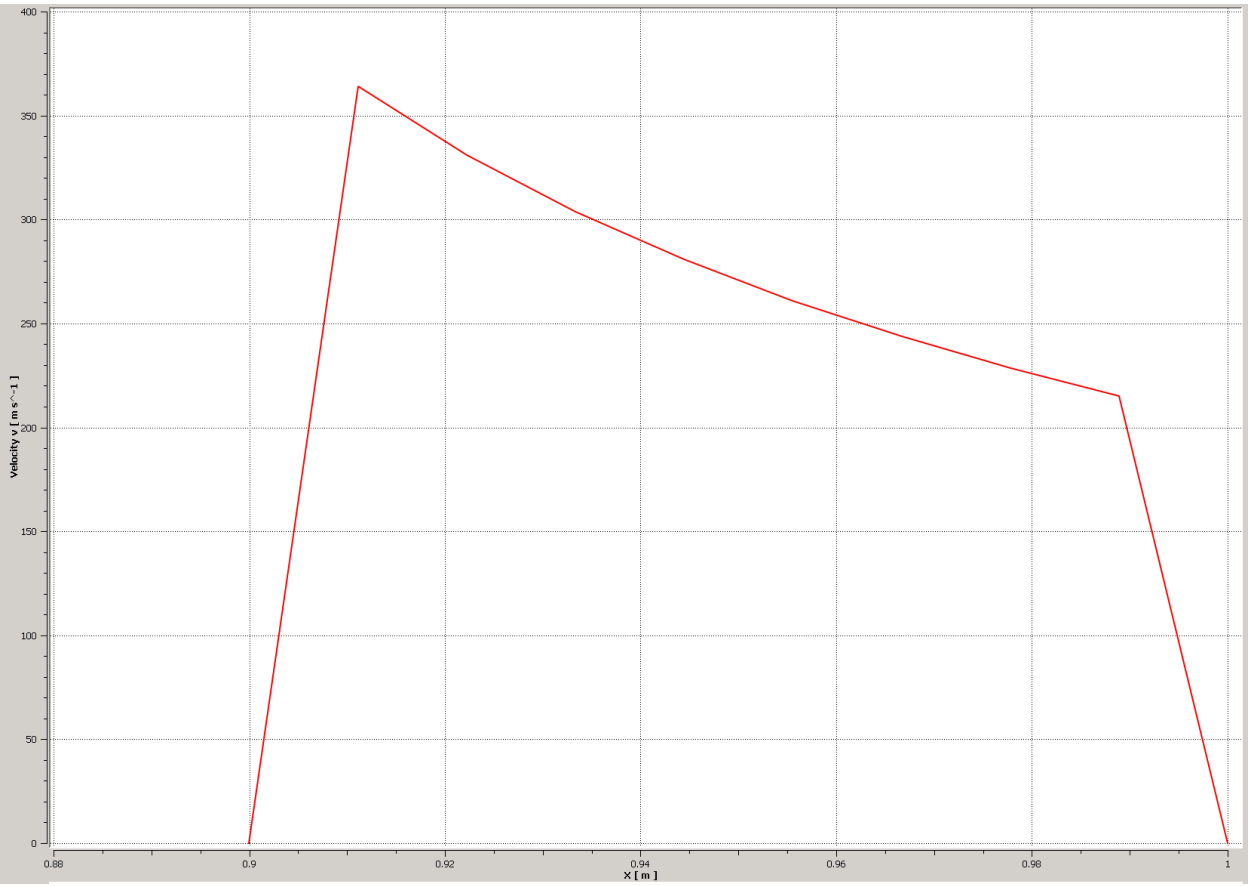

Figure 29 Inlet 4, inlet velocity versus inlet length

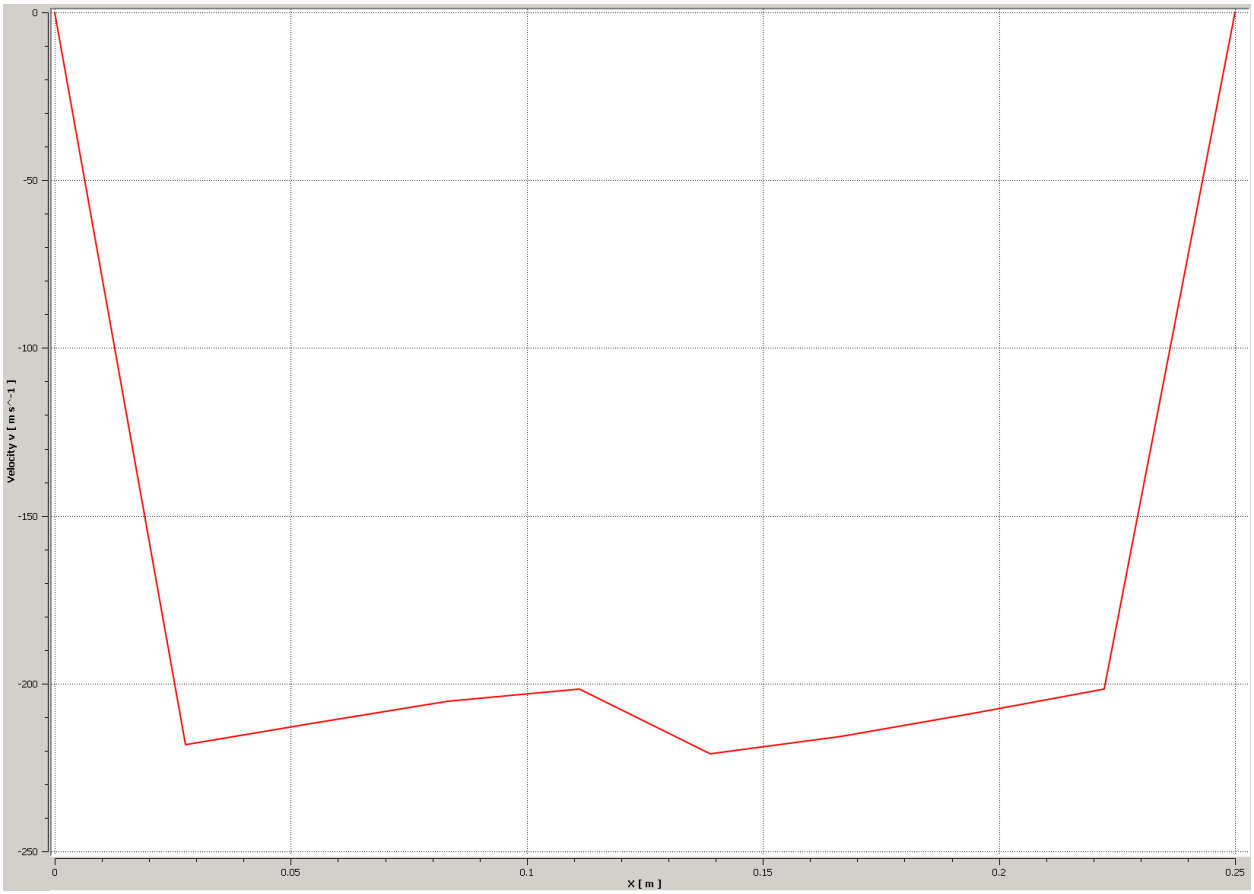

Figure 30 Outlet 1, outlet velocity versus outlet length

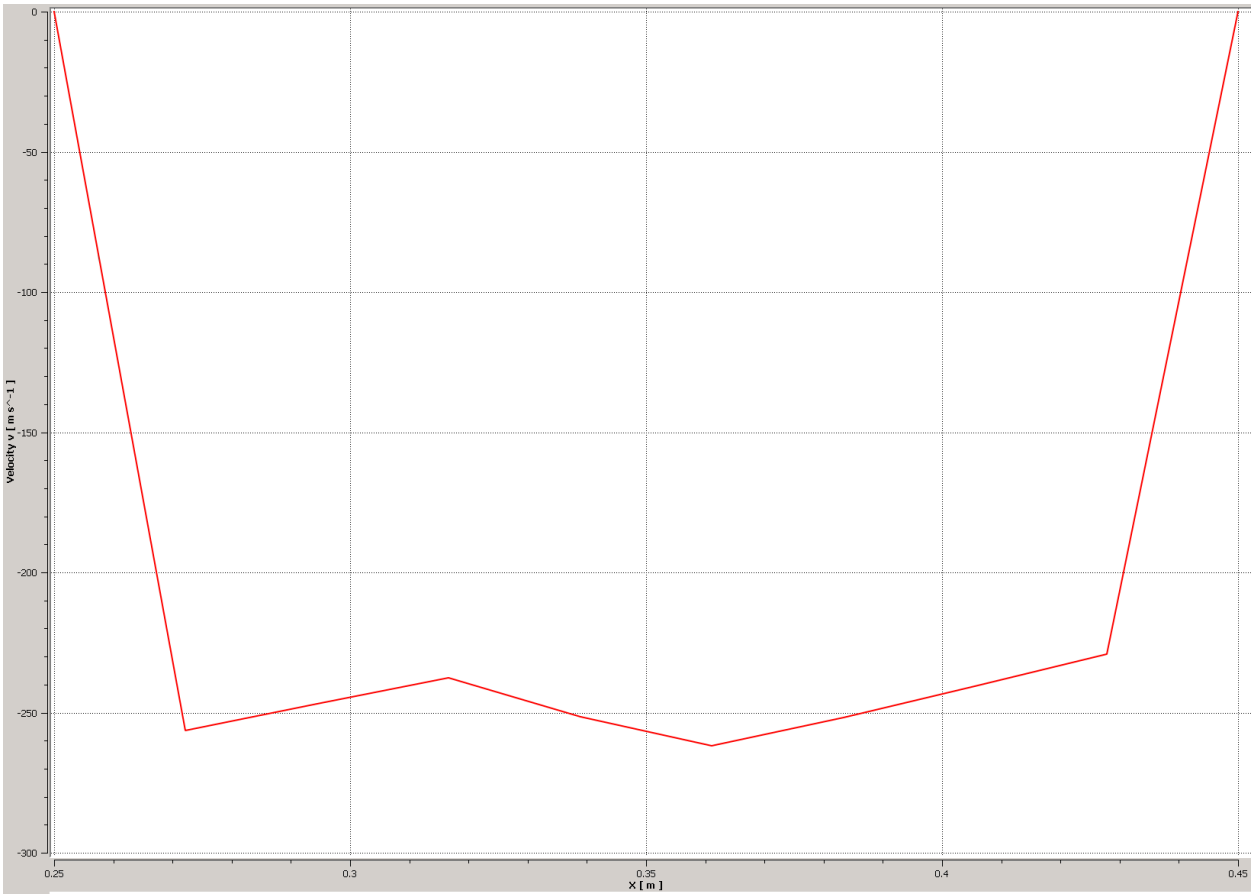

Figure 31 Outlet 2, outlet velocity versus outlet length

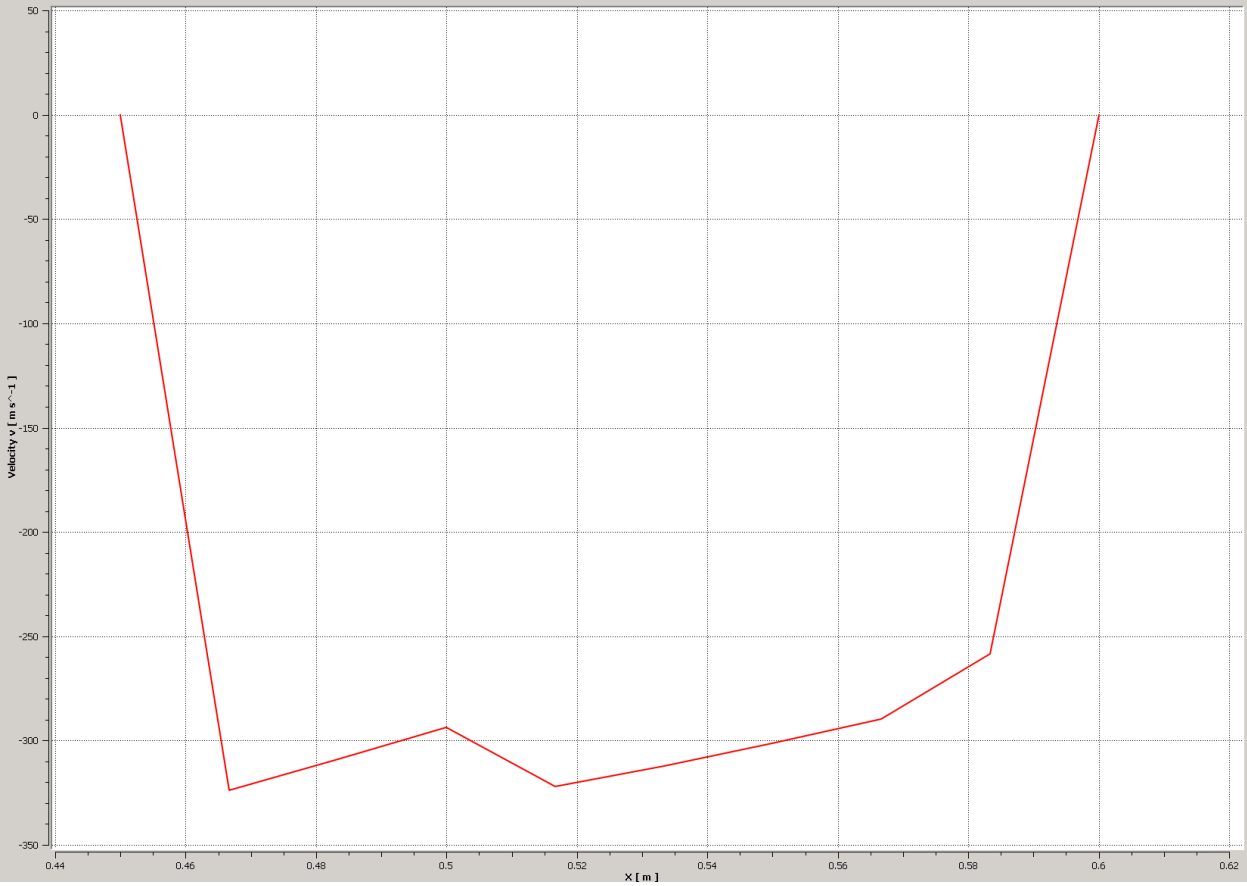

Figure 32 Outlet 3, outlet velocity versus outlet length

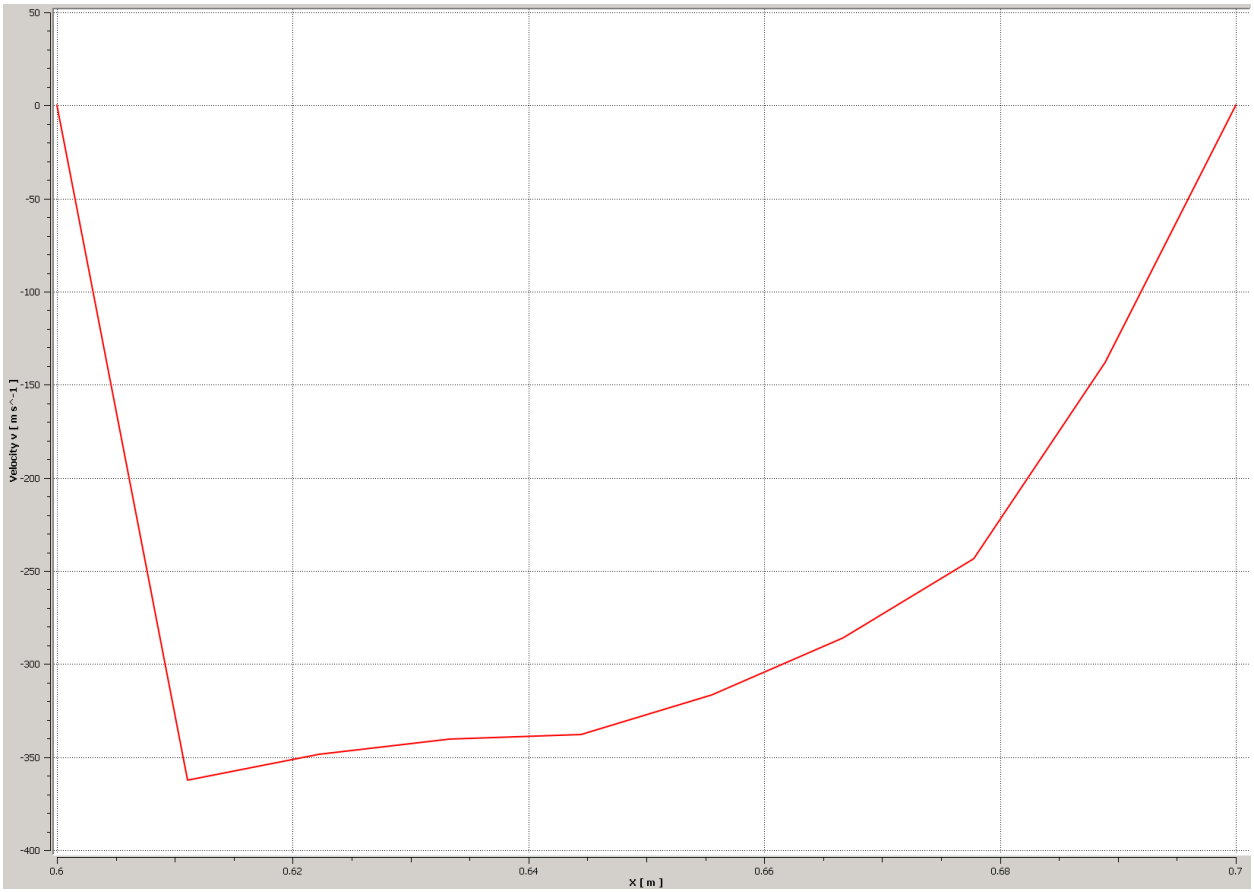

Figure 33 Outlet 4, outlet velocity versus outlet length